Research Article | Vol. 25, No. 6 | 20 Mar 2017 | OPTICS EXPRESS 7046

Optics EXPRESS

Photonic crystal microring resonator for label-free biosensing

STANLEY M. LO,[1] SHUREN HU,[2] GIRIJA GAUR,[1] YIORGOS KOSTOULAS,[1] SHARON M. WEISS,[1,2] AND PHILIPPE M. FAUCHET[1,*]

[1]*Department of Electrical Engineering and Computer Science, Vanderbilt University, Nashville, TN 37235, USA*
[2]*Department of Physics and Astronomy, Vanderbilt University, Nashville, TN 37235, USA*
[*]*philippe.fauchet@vanderbilt.edu*

Abstract: A label-free optical biosensor based on a one-dimensional photonic crystal microring resonator with enhanced light-matter interaction is demonstrated. More than a 2-fold improvement in volumetric and surface sensing sensitivity is achieved compared to conventional microring sensors. The experimental bulk detection sensitivity is ~248nm/RIU and label-free detection of DNA and proteins is reported at the nanomolar scale. With a minimum feature size greater than 100nm, the photonic crystal microring resonator biosensor can be fabricated with the same standard lithographic techniques used to mass fabricate conventional microring resonators.

OCIS codes: (050.5298) Photonic crystals; (280.1415) Biological sensing and sensors.

References and links

1. M. Iqbal, M. Gleeson, B. Spaugh, F. Tybor, W. Gunn, M. Hochberg, T. Baehr-Jones, R. Bailey, and L. Gunn, "Label-Free biosensor arrays based on silicon ring resonators and high-speed optical scanning instrumentation," IEEE J. Sel. Top. Quantum Electron. **16**(3), 654–661 (2010).
2. D. X. Xu, M. Vachon, A. Densmore, R. Ma, A. Delâge, S. Janz, J. Lapointe, Y. Li, G. Lopinski, D. Zhang, Q. Y. Liu, P. Cheben, and J. H. Schmid, "Label-free biosensor array based on silicon-on-insulator ring resonators addressed using a WDM approach," Opt. Lett. **35**(16), 2771–2773 (2010).
3. A. J. Qavi, J. T. Kindt, M. A. Gleeson, and R. C. Bailey, "Anti-DNA:RNA antibodies and silicon photonic microring resonators: increased sensitivity for multiplexed microRNA detection," Anal. Chem. **83**(15), 5949–5956 (2011).
4. K. De Vos, I. Bartolozzi, E. Schacht, P. Bienstman, and R. Baets, "Silicon-on-Insulator microring resonator for sensitive and label-free biosensing," Opt. Express **15**(12), 7610–7615 (2007).
5. F. Liang, N. Clarke, P. Patel, M. Loncar, and Q. Quan, "Scalable photonic crystal chips for high sensitivity protein detection," Opt. Express **21**(26), 32306–32312 (2013).
6. M. R. Lee and P. M. Fauchet, "Two-dimensional silicon photonic crystal based biosensing platform for protein detection," Opt. Express **15**(8), 4530–4535 (2007).
7. W. C. Lai, S. Chakravarty, Y. Zou, and R. T. Chen, "Silicon nano-membrane based photonic crystal microcavities for high sensitivity bio-sensing," Opt. Lett. **37**(7), 1208–1210 (2012).
8. C. Kang, C. T. Phare, Y. A. Vlasov, S. Assefa, and S. M. Weiss, "Photonic crystal slab sensor with enhanced surface area," Opt. Express **18**(26), 27930–27937 (2010).
9. M. R. Lee and P. M. Fauchet, "Nanoscale microcavity sensor for single particle detection," Opt. Lett. **32**(22), 3284–3286 (2007).
10. S. C. Buswell, V. A. Wright, J. M. Buriak, V. Van, and S. Evoy, "Specific detection of proteins using photonic crystal waveguides," Opt. Express **16**(20), 15949–15957 (2008).
11. R. M. Lequin, "Enzyme immunoassay (EIA)/enzyme-linked immunosorbent assay (ELISA)," Clin. Chem. **51**(12), 2415–2418 (2005).
12. T. Claes, J. Molera, K. De Vos, E. Schacht, R. Baets, and P. Bienstman, "Label-free biosensing with a slot-waveguide-based ring resonator in silicon on insulator," IEEE Photonics J. **1**(3), 197–204 (2009).
13. S. Hu, K. Qin, I. Kravchenko, S. Retterer, and S. Weiss, "Suspended micro-ring resonator for enhanced biomolecule detection sensitivity," Proc. SPIE **8933**, 893306 (2014).
14. J. Flueckiger, S. Schmidt, V. Donzella, A. Sherwali, D. M. Ratner, L. Chrostowski, and K. C. Cheung, "Sub-wavelength grating for enhanced ring resonator biosensor," Opt. Express **24**(14), 15672–15686 (2016).
15. C. Kang, S. M. Weiss, Y. A. Vlasov, and S. Assefa, "Optimized light-matter interaction and defect hole placement in photonic crystal cavity sensors," Opt. Lett. **37**(14), 2850–2852 (2012).
16. M. G. Scullion, A. Di Falco, and T. F. Krauss, "Slotted photonic crystal cavities with integrated microfluidics for biosensing applications," Biosens. Bioelectron. **27**(1), 101–105 (2011).

#285819 https://doi.org/10.1364/OE.25.007046
Journal © 2017 Received 30 Jan 2017; revised 2 Mar 2017; accepted 11 Mar 2017; published 16 Mar 2017

Optics EXPRESS

17. S. Chakravarty, Y. Zou, W. C. Lai, and R. T. Chen, "Slow light engineering for high Q high sensitivity photonic crystal microcavity biosensors in silicon," Biosens. Bioelectron. **38**(1), 170–176 (2012).
18. J. Y. Lee and P. M. Fauchet, "Slow-light dispersion in periodically patterned silicon microring resonators," Opt. Lett. **37**(1), 58–60 (2012).
19. D. Goldring, U. Levy, and D. Mendlovic, "Highly dispersive micro-ring resonator based on one dimensional photonic crystal waveguide design and analysis," Opt. Express **15**(6), 3156–3168 (2007).
20. K. McGarvey-Lechable and P. Bianucci, "Maximizing slow-light enhancement in one-dimensional photonic crystal ring resonators," Opt. Express **22**(21), 26032–26041 (2014).
21. K. McGarvey-Lechable, T. Hamidfar, D. Patel, L. Xu, D. V. Plant, and P. Bianucci, "Slow light in mass-produced, dispersion-engineered photonic crystal ring resonators," Opt. Express **25**(4), 3916–3926 (2017).
22. W. Bogaerts, R. Baets, P. Dumon, V. Wiaux, S. Beckx, D. Taillaert, B. Luyssaert, J. Van Campenhout, P. Bienstman, and D. Van Thourhout, "Nanophotonic waveguides in silicon-on-insulator fabricated with CMOS technology," J. Lightwave Technol. **23**(1), 401–412 (2005).
23. S. Pal, E. Guillermain, R. Sriram, B. L. Miller, and P. M. Fauchet, "Silicon photonic crystal nanocavity-coupled waveguides for error-corrected optical biosensing," Biosens. Bioelectron. **26**(10), 4024–4031 (2011).
24. S. Lo, S. Hu, S. Weiss, and P. Fauchet, "Photonic crystal microring resonator based sensors," in *Conference on Lasers and Electro-Optics: 2014*, OSA Technical Digest (online) (Optical Society of America, 2014), paper JTu4A.79.
25. D. Urbonas, A. Balčytis, K. Vaškevičius, M. Gabalis, and R. Petruškevičius, "Air and dielectric bands photonic crystal microringresonator for refractive index sensing," Opt. Lett. **41**(15), 3655–3658 (2016).
26. F. De Leonardis, C. E. Campanella, B. Troia, A. G. Perri, and V. M. Passaro, "Performance of SOI Bragg grating ring resonator for nonlinear sensing applications," Sensors (Basel) **14**(9), 16017–16034 (2014).
27. C. E. Campanella, F. De Leonardis, L. Mastronardi, P. Malara, G. Gagliardi, and V. M. Passaro, "Investigation of refractive index sensing based on Fano resonance in fiber Bragg grating ring resonators," Opt. Express **23**(11), 14301–14313 (2015).
28. Lumerical Solutions, Inc., *http://www.lumerical.com*.
29. X. Xu, H. Subbaraman, J. Covey, D. Kwong, A. Hosseini, and R. Chen, "Complementary metal–oxide–semiconductor compatible high efficiency subwavelength grating couplers for silicon integrated photonics," Appl. Phys. Lett. **101**(3), 031109 (2012).
30. S. Hu, Y. Zhao, K. Qin, S. Retterer, I. Kravchenko, and S. Weiss, "Enhancing the sensitivity of label-free silicon photonic biosensors through increased probe molecule density," ACS Photonics **1**(7), 590–597 (2014).
31. G. Gao, Y. Zhang, H. Zhang, Y. Wang, Q. Huang, and J. Xia, "Air-mode photonic crystal ring resonator on silicon-on-insulator," Sci. Rep. **6**(1), 19999 (2016).

1. Introduction

In the last decade, on-chip optical label-free biosensors based on optical resonant cavities have drawn a great deal of interest for delivering fast, portable, cost-effective, sensitive and accurate diagnostics [1–10]. Label-free biosensors promote simple analyte preparation and real-time monitoring of specific binding interactions by transducing the presence of specific target molecules based on their capture by surface immobilized bioreceptors, as opposed to traditional methods of labeling the target analytes with fluorescent or radiative tags [11]. Furthermore, silicon-based biosensors using the silicon-on-insulator (SOI) platform have the advantages of (1) strong light-matter interaction between resonant modes and target analytes, which increases detection sensitivity, and (2) compatibility with CMOS fabrications processes, which facilitates low-cost, compact and high quality photonic devices. Various types of optical resonant structures in silicon have been proposed and demonstrated as optical label-free biosensors such as microring resonators [1–4], one-dimensional (1D) photonic crystal (PhC) cavities [5] and two-dimensional (2D) PhC cavities [6–10]. Numerous device design approaches have been employed to further improve the sensitivity of biosensors by enhancing the light-matter interaction between target analytes and optical mode field of resonant cavities. These approaches include slot waveguide-based microring resonators [12], suspended micro-ring resonators with an enhanced evanescent field [13], sub-wavelength grating based microring resonators [14], multi-hole defect PhC micro-cavities [15], slotted PhC cavities [16] and high-Q PhC cavities [17].

In this work, a PhC microring resonator (PhCR) [18–21] is demonstrated as a label-free biosensor for specific molecular detection with enhanced detection sensitivity due to its strong light-matter interaction that results from the localized optical mode field profiles of the PhC structure. Since a fraction of the optical field in the PhCR is located inside the air holes that are accessible for molecular attachment, the PhCR can detect the presence of analyte both

Optics EXPRESS

inside the holes and on the top surface. Importantly, in contrast to slots and multi-hole defects that also support increased light-matter interaction for sensing, the critical dimensions of PhCRs are compatible with advanced deep ultra-violet (DUV) lithography [21,22], which could lead to the production of high-volume, low-cost lab-on-a-chip biosensors. Moreover, all of the important properties of conventional microring resonators as biosensors are preserved for PhCRs while a significant challenge for sensing high concentrations of molecules is removed. Like conventional microrings, PhCRs can be easily coupled to a silicon bus waveguide, enabling low optical loss, formation of sensor arrays, and error-correcting capabilities [23]. In addition, PhCRs do not have an upper limit on the concentration of analyte that can be detected due to their photonic bandgap (PBG) that gives rise to aperiodicity in the transmission resonances; the periodic transmission resonances of traditional ring resonators lead to ambiguity when measuring large spectral shifts that exceed the free spectra range. Based on the aforementioned attributes, PhCRs are promising candidates for highly sensitive biosensors in future on-chip diagnostic devices. Although the application of PhCRs as bulk refractive index sensors has been studied experimentally [24,25] and theoretically [26,27] in a few different geometries, its surface sensing capabilities have yet to be demonstrated. As a critical step toward molecular diagnostic applications, it is important that label-free biosensing experiments are shown on the PhCR platform. Moreover, previously demonstrated PhCR structures with shallow-etched holes or grating designs exhibit bulk detection sensitivities of <100nm/RIU [25,26], which are lower than those of conventional microring based sensors [1]. Therefore, in this paper, an optimized PhCR structure with stronger light-matter interaction is presented in order to demonstrate that PhCRs can achieve superior sensing performance over conventional microring resonators in both volumetric and surface sensing experiments. In the following sections, the device structure, experimental methods, and results on bulk refractive index sensitivity and label-free biosensing of DNA and protein will be presented.

2. Device structure and simulation

Figure 1(a) shows the top-view scanning electron microscope (SEM) image of the PhCR. The structure is fabricated on a SOI platform with a 220nm thick device layer. The silicon layer is etched through to the buried oxide layer. There are **N** = 100 circular air holes on the ring resonator, resulting in a ring radius of ~7.16μm. Figure 1(b) shows the magnified top-view SEM image of the device at the coupling regime. The periodicity of the air holes is **a** = 450nm, the hole radius is **r** = 0.3**a** = 135nm, the width of the ring is **d** = **a** = 450nm. The width of the coupling waveguide is **w** = 0.8**a** = 360nm or **w** = 0.75**a** = 338nm, both of which led to excellent mode matching between the input waveguide and PhCR [18]. The gap separation is **g** = 0.3**a** = 135nm, **g** = 0.4**a** = 180nm or **g** = 0.6**a** = 270nm. All of these gap separations were close to critical coupling and thus yielded high extinction ratios of the resonances. In order to give a fair comparison of sensing performance between PhCRs and conventional microring resonators, the dimensions of the fabricated control microrings are largely the same as the PhCR. The ring radius of the control microring is ~7.16μm. The width of the control microring is 450nm. The width of the coupling waveguide to the control microring is also 450nm. The gap separation between the coupling waveguide and the control microring is 100nm.

Optics EXPRESS

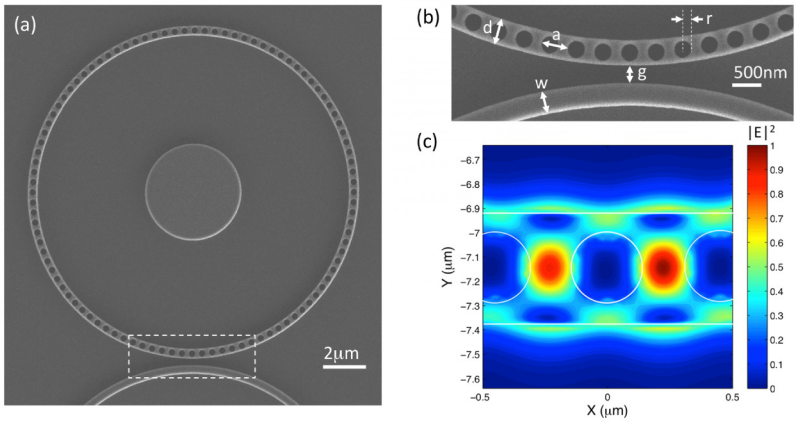

Fig. 1. (a) Top-view SEM image of the fabricated photonic crystal microring resonator. (b) Magnified SEM image of the coupling region of the PhCR (boxed region in (a)). (c) Finite-difference time-domain calculated optical mode profile when the photonic crystal microring resonator is on-resonance, which shows that a fraction of the optical field is located at the edge of air holes.

Figure 1(c) shows an example of the on-resonance optical mode field profile of the PhCR in a section of the PhC waveguide. The profile is calculated using three-dimensional (3D) finite-difference time-domain (FDTD) analysis [28]. Dimensions of the device used in the simulation are similar to the fabricated devices. The interface between Si and air regions in the PhCR structure is shown as a solid white line. The resonance wavelength is close to the photonic band gap of the structure. The polarization is TE-like (electric field parallel to the device plane). The mode profile indicates most of the optical energy is localized in the silicon region, as the resonance wavelength sits near the dielectric band edge. However, the evanescent field of the localized mode still extends to the surrounding air holes and provides enhanced modal overlap between the optical mode and the inner surface of the air holes where biomolecules can be attached. This additional active sensing area leads to an enhancement in sensitivity for PhCR as optical biosensors compared to conventional microring devices.

3. Methods

3.1 Fabrication process

Commercial SOI wafers with a 270nm device layer on top of a 3μm buried oxide (BOX) layer were used for the device fabrication. Dry-oxidation and a subsequent dip in buffered oxide etch (BOE) were performed to thin down the top silicon layer to the desired thickness of 220nm. The PhCRs and conventional microring resonators were patterned on the same chip using a single step of electron beam lithography (EBL) and a reactive-ion-etching (RIE) process. A high-resolution electron-beam photoresist (ZEP 520A) was first spin-coated on the wafer at 6000rpm for 45 seconds, which resulted in a resist thickness of ~300nm. Following a soft-bake at 180°C for 120 seconds on a hotplate, the design patterns were exposed using a JEOL JBX-9300FS EBL system. After the exposure, the wafer was developed by xylenes for 30 seconds and rinsed by IPA for 30 seconds. The wafer was then dry etched for ~2 minutes using a SF_6-based inductively-coupled-plasma (ICP) RIE etcher Oxford Plasma Lab 100, with a top silicon etch rate near 1350Å/minute. Finally the remaining photoresist on the wafer was removed by O_2 plasma in the same chamber for ~1 minute.

Optics EXPRESS

3.2 Measurement setup

Transmission spectra were measured using a wavelength scanning technique. An external-cavity continuous-wave (CW) tunable semiconductor diode laser (Santec TSL-510) was used with a wavelength tunable range from 1510nm to 1630nm. The output laser beam was guided by a single-mode optical fiber (SMF) to a polarization controller to adjust the output polarization. The output polarization was TE-like in all experiments and was calibrated using a free space polarization beam-splitter and photodetector. The laser beam was then coupled to the device through a 10° tilted cleaved-end SMF and an input grating coupler on the sample that was fabricated alongside the PhCR structure. The grating coupler design reported in [29] was followed with appropriate modification of the dimensions for devices on 220nm thick SOI. The output signal from the output grating coupler was collected by a cleaved-end SMF. The positions of the SMFs and sample were controlled by translation stages. A long working distance lens and visible-light CCD camera on top of the sample monitored the alignment of the sample and fibers. The transmission intensities were measured by a photodetector and recorded by a computer.

3.3 Surface functionalization

For experimental demonstration of surface-based DNA label-free biosensing, a protocol similar to that reported in [30] was followed to attach DNA to the PhCR. First, the sample was oxidized in air at 500°C for 10 minutes to ensure that the appropriate surface passivation and surface chemistry was obtained for subsequent functionalization steps. Next, 3-aminopropyltriethoxysilane (3-APTES) was diluted in anhydrous toluene to a concentration of 2%, and the sample was soaked in the resulting solution for 15 minutes to achieve an amine terminated surface functionalization. Thereafter, the sample was flushed with ethanol and DI water several times and cured inside an oven at 150°C for 20 minutes. A linker molecule, succinimidyl 3-(2-pyridyldithio)propionate (SPDP), was dissolved in HEPES buffer, and the sample was then soaked in the solution for 2 hours, followed by a 1 hour HEPES buffer soak to remove any unbound molecules. An excess (100μM) of 16-mer probe DNA in HEPES buffer was mixed 1:1 by volume with disulfide reducing agent TCEP in DI water and ethanol for 30 minutes and then pipetted onto the sample. After 1 hour incubation at 37°C, the sample was soaked in HEPES buffer for 20 minutes at 37°C, rinsed with DI water, and dried with nitrogen gas to remove any remaining unattached molecules. Finally, a 16-mer single-stranded target DNA at a concentration of 500nM was attached to the sample. We note that the PhCR and control microring devices were exposed to identical functionalization processes and experimental conditions for all experiments to enable a direct comparison of their biosensing performance.

For the experimental demonstration of label-free protein detection, the following protocol was followed to attach proteins to the PhC microring biosensor. First, the oxidized samples were immersed in a freshly prepared piranha solution for 15 minutes to remove organic surface contaminants and ensure a chemically clean surface. Following piranha clean, the samples were rinsed thoroughly with copious amounts of water and dried under nitrogen. Then, 50μL of freshly prepared 2% 3-APTES solution in anhydrous toluene was drop cast onto each sample for 15 minutes to provide an amine functionalized surface. The excess unreacted 3-APTES was thoroughly rinsed from the samples three times with ethanol and DI water. The samples were then dried under nitrogen flow and baked in an oven at 100°C for 20 minutes to enable the formation of stable 3-APTES cross-links. Next, 50μL of a 200μM biotin solution in phosphate buffer saline (PBS) buffer was pipetted onto each sample and incubated for 1 hour. Unattached biotin molecules were washed away by rinsing the samples with DI water and ethanol, then drying under nitrogen. The samples with covalently bound biotin probe molecules were then sequentially exposed to 50μL of varying concentrations (20nM, 100nM, 200nM) of target streptavidin molecules solvated in PBS solutions for 1 hour. Excess streptavidin molecules were washed away from the sample surface by thorough DI

Optics EXPRESS

water and ethanol rinse steps. The samples were then dried under nitrogen. Note that for all experiments, the same sample was exposed to increasing streptavidin concentrations without removing the already captured streptavidin molecules.

4. Results and discussion

4.1 Bulk index sensitivity

Figure 2(a) shows a typical transmission spectrum of the PhCR-based biosensor. The wavelength resolution is 5pm. The incident power is fixed at 1mW for all experiments. In the spectrum, there are no resonances below about 1550nm due to the PBG. Above 1550nm, there are multiple resonance dips with highly non-uniform free spectral ranges (FSRs). The FSR between resonance peaks decreases from ~12nm at ~1595nm to ~3nm at ~1555nm. The reduction of FSRs close to the band-edge of the PBG is due to the slow-light effect of the PhC waveguide embedded in the microring. The calculated group index is ~17 ($\mathbf{n_g} \approx \lambda^2/\delta\lambda L$ where L is the circumference of the PhCR). For the control microring resonator, the FSR between resonance peaks is ~11.5nm across the entire optical spectrum. This uniform FSR shows a linear dispersive characteristic, and the calculated group index is ~4.6 at 1555nm. Note that the slow light effect for the PhCR does not directly contribute to its increased detection sensitivity because the increased group index results in both an increase of the phase change in the PhCR and a decrease in the FSR. The extinction ratio of the resonance mode in the PhCR next to the photonic band edge is ~10dB, which suggests a nearly critical coupling condition of the resonator is achieved. However, the loaded quality factor Q_{load} of the same mode is ~1200, which is less than that of our previously fabricated PhCRs (Q_{load} ~2500) [18]. The lower Q_{load} of this PhCR compared to previously fabricated PhCRs may be due to fabrication imperfections and enlarged air hole dimensions in these specific devices for biosensing applications. The enhanced modal overlap at the silicon-air interface also increases the magnitude of scattering losses that result from surface roughness produced during the silicon reactive ion etching process in the fabrication. The control mircroing exhibits a loaded quality factor of ~35,000 and an extinction ratio of ~15dB for the resonance at 1555nm.

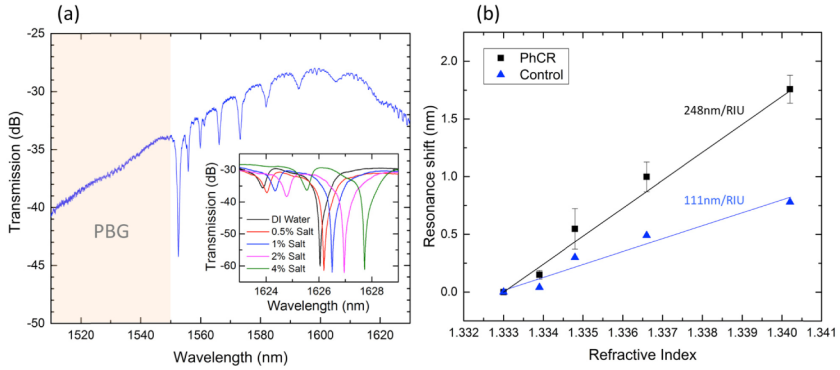

Fig. 2. (a) Measured TE-polarized transmission spectrum of the PhCR. PBG: photonic band gap. (Inset) Measured transmission spectra of PhCR exposed to DI water and different concentrations of salt water solution. Resonances are red shifted when salt concentration is increased. (b) Resonance shifts of PhCR and control microring exposed to different concentrations of salt water solution. The solid lines are linear fits to the data.

In order to obtain the bulk refractive index sensing performance of the PhCR, the PhCR along with a conventional microring resonator were exposed to salt water solutions with different NaCl concentrations. In the experiment, 0%, 0.5%, 1%, 2% and 4% concentration solutions were used. The transmission measurements of the PhCR and control microring devices were immediately started once the solutions were applied on the sample. The samples were rinsed by DI water and dried with nitrogen gas between measurements, before the next

Optics EXPRESS

salt water solution was exposed to the samples. After rinsing, the resonance wavelength returned to its initial condition, confirming that no salt residue remained in the samples. The inset of Fig. 2(a) shows the measured transmission spectra of the PhCR exposed to DI water and different concentrations of salt water solution. The results indicate the resonance dips red shift when salt concentration is increased. Figure 2(b) summarizes the resonance shifts of the PhCRs and control, conventional microring resonators as a function of the refractive index of the applied salt water solution. Linear fits to the data show that the PhCR has an experimental bulk refractive index sensitivity of ~248nm/RIU, while the control microring has a sensitivity of ~111nm/RIU. Note that the bulk sensitivity of the control microring is similar to what has been previously reported [1]. The more than 2-fold increased bulk detection sensitivity of the PhCRs compared to the control microring is largely due to the increased area for light-matter interaction between the guided mode and salt water solution exposed to the rings.

4.2 Experimental demonstrations of label-free biosensing of DNA molecules

In order to examine the surface-sensing capabilities of the PhCR, label-free biosensing experiments were first carried out using the specific attachment of DNA molecules. Figure 3(a) shows the measured TE-polarized transmission spectra of the PhCR after each step of the surface functionalization processes and after capture of the target DNA molecules. After oxidation of the sample that blue shifts the resonance (not shown), the resonance wavelength red shifts after each molecular attachment step as a thin layer of biomolecules functionalized on the PhCR surface increases the effective refractive index of the PhCR. Figure 3(b) summarizes the resonance wavelength changes of the PhCR and the control microring resonator after each step of the DNA sensing experiment. The resonance shifts of the PhCR after (a) 3-APTES, (b) SPDP linker, (c) 100μM probe DNA and (d) 500nM target DNA are (a) 0.32nm, (b) 0.22nm, (c) 0.79nm and (d) 0.16nm, respectively. The resonance shifts of the control microring are (a) 0.1nm, (b) 0.1nm, (c) 0.27nm and (d) 0.08nm, respectively. These results show that the PhCR has a more than 2-fold enhancement in surface sensing sensitivity compared to the control microring for every step of the DNA sensing experiment. The magnitude of this performance enhancement is consistent with the bulk index sensitivity results reported in the previous section.

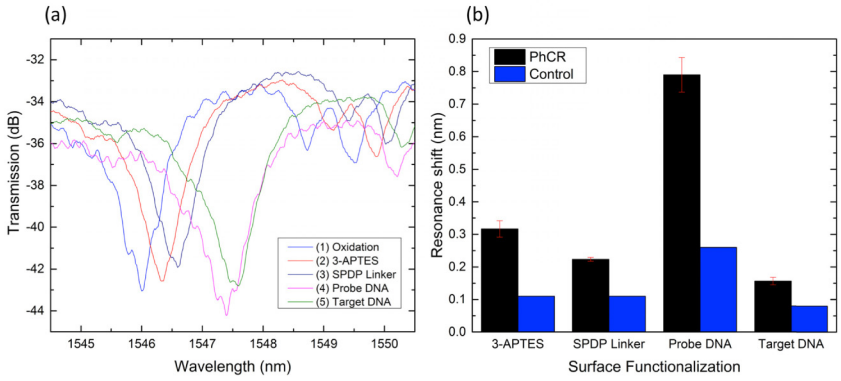

Fig. 3. (a) Measured TE-polarized transmission spectra of a PhCR after various surface functionalization steps and after exposure to 500nM target DNA. (b) Resonance red shifts for PhCR and control microring resonators for each step of the DNA detection experiment. Three PhCRs were tested in the experiments.

4.3 Experimental demonstrations of label-free biosensing of protein molecules

In addition to the DNA surface sensing experiment, a label-free biosensing experiment with proteins was carried out to further demonstrate the surface sensing capabilities of the PhCR

Optics EXPRESS

and to verify the previous experimental results. Figure 4(a) shows the measured TE-polarized transmission spectra of the PhCR after each step of the surface functionalization processes and after capture of various concentrations of the target protein, streptavidin. As expected, the resonance red shifts after each step of the process due to the increase in effective refractive index of the PhCR that results from the molecular attachments. Figure 4(b) summarizes the resonance wavelength changes for the PhCR and conventional microring resonator during the protein sensing experiment. The resonance red shifts of the PhCR after (a) 3-APTES, (b) 200μM biotin, (c) 20nM streptavidin, (d) 120nM streptavidin and (e) 320nM streptavidin are (a) 1.23nm, (b) 0.81nm, (c) 0.18nm, (d) 1.77nm and (e) 2.42nm, respectively. The resonance red shifts of the control microring are (a) 0.58nm, (b) 0.25nm, (c) 0.08nm, (d) 0.75nm and (e) 1.23nm, respectively. The data suggest that most, if not all, biotin probes are hybridized with streptavidin targets at a streptavidin concentration between 120 and 320nM, which is consistent with prior work [30]. Similar to the DNA surface sensing experiment, the protein sensing experiment shows that the PhCR has more than a 2-fold enhancement in detection sensitivity compared to the control microring for every molecular attachment step. Note that a larger resonance shift was experienced after 3-APTES attachment in the protein experiment. Based on prior work [30], it is expected that an incomplete monolayer of 3-APTES was formed in the DNA sensing experiments; however, the same relative coverage was likely formed on both the PhCR and the control microring such that a fair comparison of sensing performance took place. It is also possible that slightly more than a single layer of 3-APTES molecules was attached in the protein experiments but, again, the same conditions were applied to the PhCR and control microring ensuring the integrity of the sensing comparison. Given that the additional air holes present in the PhCRs led to an increase of only ~32% in total accessible surface area for molecular attachment (i.e., at the Si-air interfaces) compared to the control microring, the 2-fold detection sensitivity enhancement in both bulk sensing and surface sensing experiments indicates that the optical mode profile, and more specifically the evanescent field in the photonic crystal air holes, plays a significant role in the measured sensitivity enhancement. We note that the similar enhancement for bulk and surface sensing is consistent with the field distribution shown in Fig. 1(c), which shows that the field enhancement in the air holes occurs near the Si-air-interface; hence, no additional sensitivity enhancement is experienced by analyte that fills the holes compared to analyte that only binds on the surface of the holes. The experimental results reported here are based on a PhCR with resonances near the dielectric band edge; it is expected that an even higher sensitivity may be obtained if a resonance near the air band edge is used [25,31].

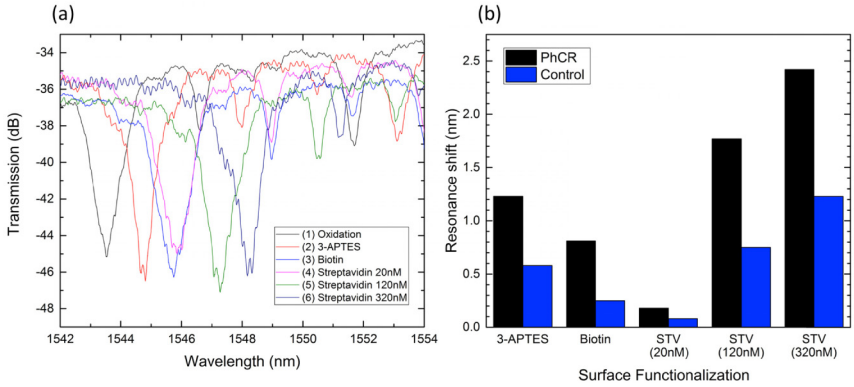

Fig. 4. (a) Measured TE-polarized transmission spectra of the PhCR after various surface functionalization steps and after exposure to various concentrations of target proteins. (b) Resonance red shifts for PhCR and control microring resonators for each step of the protein detection experiment. STV: streptavidin.

Optics EXPRESS

5. Conclusion

The detection sensitivity of PhCR-based biosensors due to bulk refractive index changes and specific DNA and protein binding was investigated. The bulk refractive index change detection sensitivity of PhCRs is ~248nm/RIU, which is more than 2-fold greater than that of conventional microring devices. Label-free biosensing of DNA and protein at the nanomolar scale also revealed that PhCRs have a more than 2-fold surface sensing detection enhancement over conventional microring devices. The detection sensitivity enhancement is attributed to the increased light-matter interaction area where the guided mode of the PhCRs interacts with target analyte. With the advantages of high sensitivity, CMOS compatibility and efficient coupling to existing silicon photonics platforms, PhCRs are promising candidates as optical biosensors in future on-chip diagnostic devices.

Funding

National Science Foundation (NSF) (ECCS1407777, ECCS1542174).

Acknowledgments

Electron beam lithography was performed at the Georgia Tech Institute for Electronics and Nanotechnology, a member of the National Nanotechnology Coordinated Infrastructure. Dry-oxidation, photoresist processing and reactive-ion-etching were carried out at the Center for Nanophase Materials Sciences, which is a DOE Office of Science User Facility. The authors thank S. T. Retterer, D. P. Briggs and I. K. Kravchenko for assistance with sample fabrication.